Research Article | **Open Access**

Encapsulation of Water Insoluble Drugs in Mesoporous Silica Nanoparticles using Supercritical Carbon Dioxide

A. Patil[1]*, U. N. Chirmade[1], Vivek Trivedi[1], D. A. Lamprou[2], A. Urquhart[2] and D. Douroumis[1]

[1]Medway School of Science, Department of Pharmaceutical Sciences, University of Greenwich, Chatham Maritime ME4 4TB, Kent, United Kingdom
[2]Strathclyde Institute of Pharmacy and Biomedical Sciences, University of Strathclyde, The john Arbuthnott Building, Glasgow, G4 0NR, Scotland

Abstract

Mesoporous silica nanoparticles MCM – 41 were synthesized with two dimensional hexagonal p6mm symmetry, high specific surface area(~ 980m^2/g) narrow pore size and an average particle size of 186 nm. The produced nanoparticles were used to encapsulate carbamazepine through a supercritical carbon dioxide process combined with various organic solvents. Supercritical processing was found to provide increased drug encapsulation. The loaded MCM - 41 nanoparticles were analyzed using X–ray diffraction and differential scanning calorimetry (DSC) to investigate the crystalline state of the encapsulated carbamazepine and it was found to be dependent on the nature of the organic solvent. Carbamazepine showed increased dissolution rates under sink conditions. Viability studies of Caco – 2 cells demonstrated negligible cytotoxicity for the MCM–41 nanoparticles.

Introduction

Mesoporous silica nanoparticles (MSNs) have attracted the attention of several scientists over the last decade due to their potential applications. Among the main features of mesoporous materials is the high surface area, pore volume and the highly ordered pore network which is very homogeneous in size. As a result of these features MSNs are excellent candidates as drug delivery systems. MSNs can be synthesized either by an alkaline route [1] or an acid route [2] both using surfactants as templates. Under alkaline conditions the silica precursors are negatively charged and they interact with the positively charged surfactants via electrostatic interactions. The silica species therefore polymerize at the micelle surface, thereby creating a negatively charged silica surface. Subsequently, surfactants are self–assembled into the structure that best matches the silica surface. By removing the surfactants an ordered stable, porous structure with high surface area is created.

Initially, MSNs were discovered by Mobil scientists [1,3] designated as MCM–41 or MCM–48 and used as molecular sieves. However, for first time MSNs were used as drug delivery system by Valet–Regi [4] to encapsulate Ibuprofen in MCM–41 of various pore sizes. In several occasions MSNs have been reported to control the release profile or to enhance the solubility of various active substances [5,8]. The MSNs pore size can be designed slightly larger than the dimension of the drug molecule and thus to provide sustained release for several hours [9]. In addition, MSN present high drug loading capacities ranging from 10 to 34% [10] or even to 60% in rare cases [11]. The presence of surface silanol groups facilitates MSN's functionalization [12,14] by various groups (hydroxyl, amine, thiol, carboxyl) which can then conjugated with fluorophores and target ligands for optical imaging of tumour cells *in vitro*. MSNs have been also used as drug delivery systems of both water insoluble [15] and water soluble anticancer agents [16] by providing controlled release in the cell compartments.

In the current study we investigated the encapsulation of carbamazepine (CBZ) in MCM–41 nanoparticles by using supercritical CO_2 processing. The CO_2 process has been previously employed to load silica aerogels [17–20]. Initially, Smirnova et al. (2004) reported that CO_2 was successfully used to load various active substances in hydrophilic and hydrophobic aerogels leading to increased loading efficiencies. In later studies, the same group investigated the adsorption of various organic molecules as a function of crystallization, surface properties and surface interactions. Nowadays, about 40% of small–molecule drugs in the pipeline of the pharmaceutical companies present low water solubility [21,22] and therefore it is difficult to formulate. Carbamazepine is a major antiepileptic pharmacological agent with low water solubility (13mg/100mL) and its inclusion in MCM–41 is expected to increase dissolution rates. Currently, drug loading of MSNs is conducted by using various approaches such as solvent, incipient wetness impregnation and melt methods to enhance drug loading in pore channels [23]. Herein, supercritical fluid processing is introduced as a reproducible, controllable and scalable alternative for drug loading. In addition, we report the effect of CO_2 processing on the crystallinity of the active substance and how this could induce changes on the polymorphic CBZ forms.

Materials and Methods

Materials

Carbamazepine was kindly donated by Novartis Pharma (Basel, Switzerland). Tetraethyl Orthosilicate (TEOS) and hexadecyltrimethylammonium bromide (CTAB) were obtained from Sigma Aldrich (St. Lewis, US). The HPLC grade solvents acetone, methanol, ethanol were purchased from Fisher Chemicals (Karlsruhe, UK). All materials were used as received.

Synthesis of mesoporous silica nanoparticles

CTAB (0.5g) 2.0M NaOH (1.75ml) and deionised water (120g)

were heated at 80°C for 30 minutes to reach a P^H of 12.3 To this clear solution TEOS (2.34gm) 2.5ml is rapidly injected via injection under vigorous stirring. Following the injection a white precipitation will be observed within three minutes of stirring at 550 rpm. The reaction temperature is maintained at 80°C for 2 hours. The product is isolated by hot filtration washed with copious amount of water and methanol (5ml each for three times). An acid extraction was performed in a methanol (100 mL) mixture of concentrated hydrochloric acid (1.0 mL) and as-made materials (1.0 g) at 60C for 6 h. The surfactant-removed solid products were filtered and washed with water and methanol, and then dried under vacuum.

Drug encapsulation

The process used for the CBZ encapsulation in mesoporous silica nanoparticles was conducted in a high pressure R250 CW reactor (Thar Technologies Inc. USA). CBZ was dissolved in various organic solvents
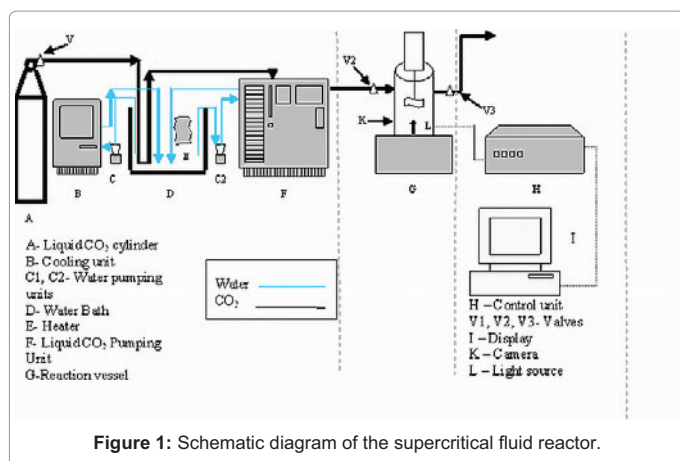
Figure 1: Schematic diagram of the supercritical fluid reactor.
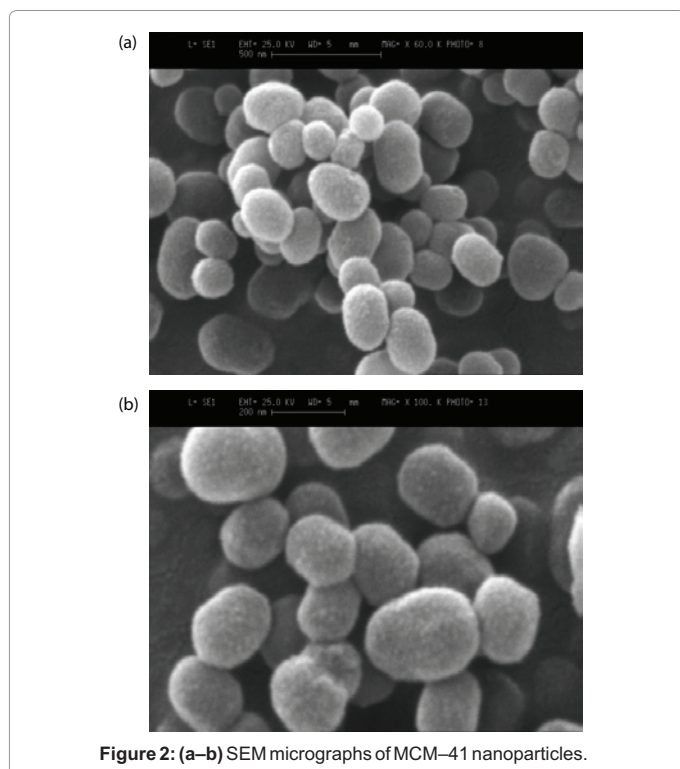
Figure 2: (a–b) SEM micrographs of MCM–41 nanoparticles.
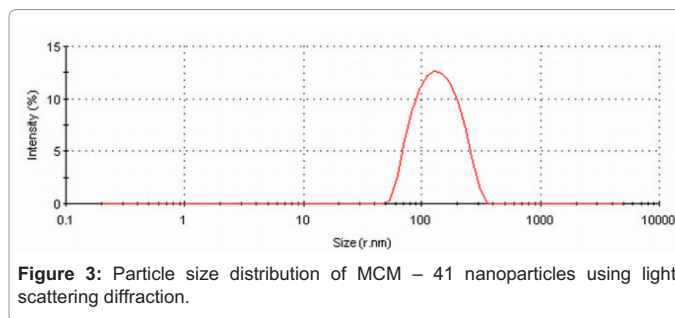
Figure 3: Particle size distribution of MCM – 41 nanoparticles using light scattering diffraction.

following mixing with supercritical CO_2 into the high pressure vessel to reach the operating conditions of pressure (150 bars) and temperature (70°C). The contents of the vessel were then mixed with a paddle stirrer for 1 hr under the operating conditions before decompression of the vessel and removal of the drug encapsulated nanoparticles. After a 1 hr decompression cycle the organic solvent flushed out by feeding CO_2 simultaneously. Figure 1 depicts a schematic diagram of the high pressure reactor.

Determination of loading efficiency

The loading efficiency of MCM–41 was determined by adding 50 mg of loaded samples in 20 ml ACN and stirred for 24 hr. The samples were centrifuged in a Sorval RC6 Plus centrifuge at 7000 rpm for 30 min. The supernatant was collected and determined with HPLC analysis.

Particle size measurements

The particle size of the dispersions was measured with Malvern Masterisizer 2000 (Malvern, UK) combining information from simple light scattering (LS) and polarization intensity differential scattering (PIDS). For data evaluation, an optical model based on the Mie theory was created using the instrumental software assuming 1.45 as the real and 0 as the imaginary part of the refractive index of the particles. Results given are the mean of 5 successive measurements of 120 s each.

Scanning Electron Microscopy (SEM)

The morphology of newly synthesized MCM–41 was examined by scanning electron microscopy. The samples were attached to aluminum stubs with double side adhesive carbon tape then gold coated and examined using a scanning electron microscope (Jeol 5200, SEM).

Transmission Electron Microscopy (TEM)

TEM carried out with a JEOL JSM200CX operating at 200kV accelerating voltage. Briefly, 1 μL of nanoparticles was placed onto a 400 mesh Cu grid with a carbon film support and excess liquid was blotted from beneath the grid and then left to air dry. Images were captured using a bottom mounted Gatan Orius SC200 ccd camera with Digital Micrograph software. The magnifications were calibrated using 8.75nm lattice spacing of catalase crystals.

Differential scanning calorimetry

The physical state of the pure drugs and the loaded MCM–41 samples were examined by differential scanning calorimetry (DSC). The thermographs of each powder were obtained by using a Mettler Toledo 823e (Greifensee, Switzerland) differential scanning calorimeter. Samples accurately weighted (2–3 mg) were placed in pierced aluminium pans and heated from 20 to 260°C at a scanning rate of 10°C min^{-1} in a nitrogen atmosphere.

Atomic Force Microscopy (AFM)

For AFM experiments, 50 μL of silica particles which were suspended in toluene (99 %; Fisher Scientific, Loughborough, UK), was deposited onto a freshly cleaved mica surface (G250-2 Mica sheets 1" x 1" x 0.006"; Agar Scientific Ltd, Essex, UK), and dried under ambient conditions for 5 h. The images were obtained by scanning the mica surface in air under ambient conditions using a Veeco MultiMode with NanoScope 3D Controller Scanning Probe Microscope (Digital Instruments, Santa Barbara, CA, USA; Veeco software Version 5.31r1) operated in tapping mode. The AFM measurements were obtained using soft silicon probes (FESP; nominal length (l_{nom}) = 225 μm, width (w_{nom}) = 28 μm, tip radius (R_{nom}) = 8 nm, resonant frequency (v_{nom}) = 75 kHz, spring constant (k_{nom}) = 2.8 N m^{-1}; Veeco Instruments SAS, Dourdan, France). AFM scans were taken at 512 x 512 pixels resolution and produced topographic images of the samples in which the brightness of features increases as a function of height. Typical scanning parameters were as follows: tapping frequency 71 kHz, integral and proportional gains 0.2 and 0.3, respectively, set point 0.7–1.0 V and scanning speed 1.0 Hz. These experiments were repeated two times in fresh mica in 6 different areas. The images were analyzed by using Veeco Image Analysis software Version 6.14r1.

BET analysis

BET surface area, pore volume and pore diameter of MCM–41 was measured by using Micromeritics Gemini 6 (Norcross, USA) automated gas sorption system model. The determination of micropore volume, micropore surface area, and external surface area was estimated by using the standard t–plot calculations, while the pore size and distribution was estimated using Broekhoff and de Boer (BdB) reports.

Dissolution studies

The release of CBZ from loaded m-SiNPs samples carried out in 750 ml of 0.1 M hydrochloric acid for 2 hr using a Varian 705 DS dissolution paddle apparatus (Varian Inc. North Carolina, US) at 100 rpm and 37 ± 0.5°C. After 2 hr operation, 250 ml of 0.20 M solution of trisodium phosphate dodecahydrate were added into the vessel (buffer stage, P^H 6.8) that has been equilibrated to 37C. At predetermined time intervals samples were withdrawn for HPLC assay. All dissolution studies were performed in triplicate.

HPLC Analysis

The concentration of drug in the samples was determined by HPLC. An Agilent 1200 Series (Waldbronn, Germany) equipped with a multiple wavelength detector (MWD) and a Beckman - Coulter Nucleosil 100 RP, $5\mu m$ X 4.5 mm X 25 cm column was used for HPLC assay. Mobile phase contained ACN/water/phosphoric acid at a ratio of 49.9:49.9:0.2v/v. The mobile phase was left to stand for at least 12 h. The flow rate was 1.0 mL min^{-1} and the injection volume was $20\mu L$ while column temperature maintained at 25°C. The wavelength was monitored at 236 nm and calibration curves were constructed using standard solutions of known concentrations from 5μg/mL to 50μg/mL. The Agilent software calculated the peak area of each standard solution and sample automatically.

Cytotoxicity studies

Viability of intestinal Caco-2 cells was evaluated using MTT assay, which is associated to cell mitochondrial activity. The assay is based on the ability of viable cells to convert thiazolyl blue tetrazolium bromide solution to the blue formazan crystals in their mitochondria
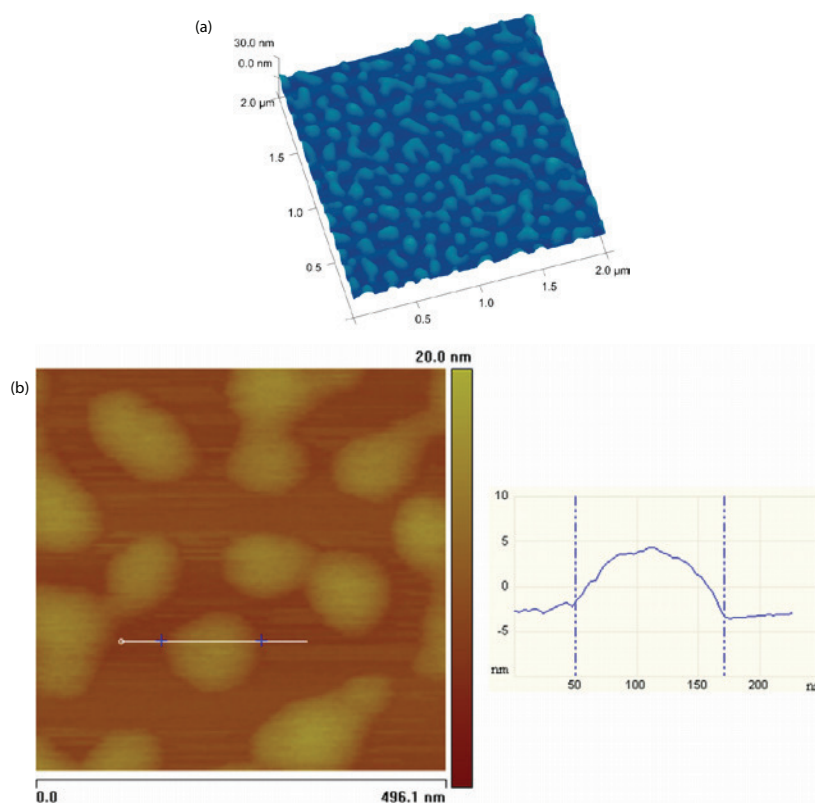

**Figure 4: (a – b)** AFM images of MCM–41.
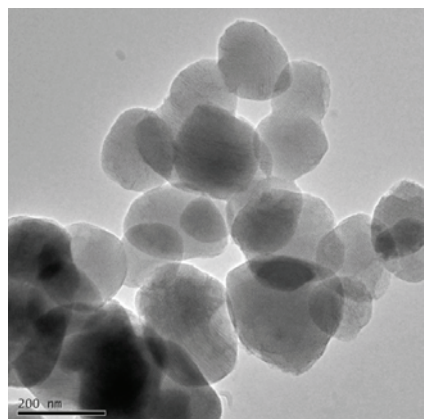
**Figure 5:** Transmission electron micrograph of MCM–41 nanoparticles.
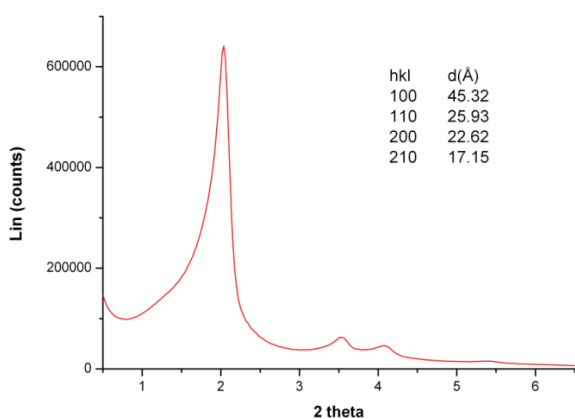
Figure 6: X – ray diffractogram of pure MCM–41 nanoparticles synthesized by the sol – gel process.
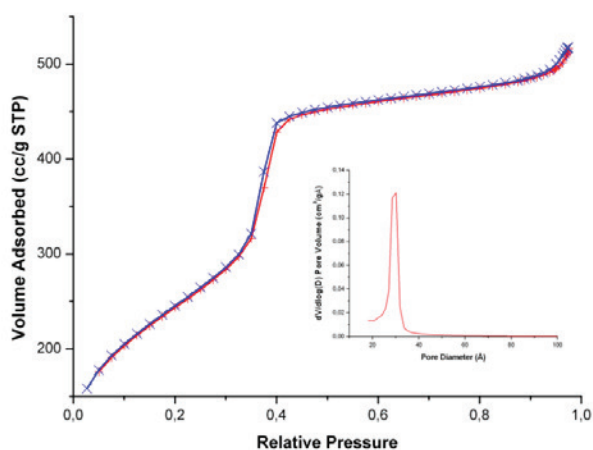

Figure 7: Nitrogen adsorption isotherm for synthesized MCM–41. The inset image shows the pore size distribution.

[24]. Briefly, the cells were seeded at a concentration of 5×10^4 cells/mL/ well in 24-well plates and were incubated with silica nanoparticles at increasing concentrations for 1 day. The cells in the first three wells were incubated in the absence of the formulation. DMSO (0.5 mL/well) was used as positive control for cell death.

After 24 hrs of incubation, 100 μL of MTT solution (concentration 5 mg/mL) was added to the wells and incubated for two hours at 37°C. The blue formazan salts were dissolved in 100 μL of acidified isopropanol (0.33μL HCl in 100 mL isopropanol), which was transferred to 96-well plates and the absorbance was read on a microplate reader (Bio-Tec Instruments) at wavelength of 490 nm. Cell viability was calculated by comparing the number of viable cells in the formulation-treated wells to the non-formulation treated cells.

Results and Discussion

Silica synthesis and characterization

MCM–41 nanoparticles were prepared by the sol–gel process using CTAB as the structure directing agent similar to Huo et al. [2]. The process carried out in alkaline media above the isoelectric point of silica where the silica precursors will be present as anionic species. As a result silica species precipitate and lead to intermediate mesophases through a (S^+I^-) route where S^+ is the cationic surfactant and I^- is the deprotonated Si–OH moiety. By altering the molar ratio of CTAB (1–2.5) and the processing times it is possible to control the obtained MCM–41 particle size and hence the surface area, the pore volume and the pore size (not shown). The morphology of the produced nanoparticles was studied by SEM, AFM and TEM analysis.
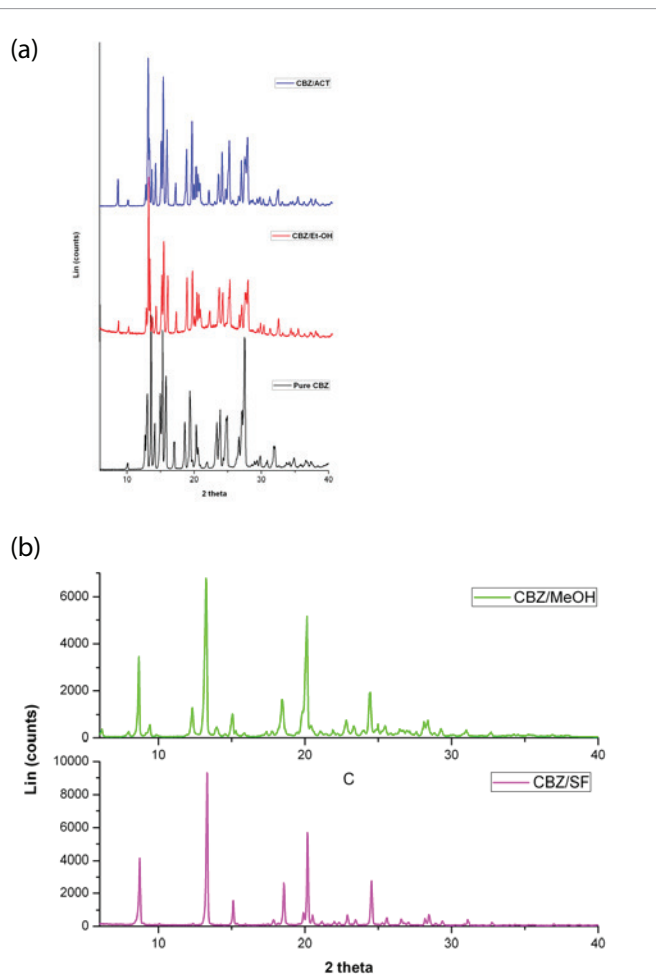

Figure 8: XRD patterns of a) CBZ loaded MCM – 41 nanoparticles process by acetone, ethanol – pure CBZ (bottom) and b) methanol and control (processed only with CO_2).

In Figure 2 the SEM micrographs displayed relatively uniform particle size distribution of approximately 200nm with a spherical shape. It can be seen that particles are almost spherical with a rough surface. The particle size was accurately estimated by dynamic light scattering measurements (Figure 3) and it was found to be 186nm (polydispersity index 0.522). The particle size distribution could be an issued for the synthesis of MCM-41 nanoparticles as they present high poyldispersity index. Nevertheless, there are reports where synthesized silica nanoparticles demonstrated narrow particle size distributions [25]. In our case the obtained particle size was reproducible under the conditions followed for the MCM-41 synthesis. In addition, nanoparticles were further characterized by atomic force microscopy studies [26] to image the shape and the appearance of pure MCM–41. As shown in Figure 4 (a,b) AFM can efficiently resolve surface details in the nanometer scale by producing three dimensional images of the MSN samples. The MCM–41 can be clearly seen as spherical

particles with 200 nm diameter, very high homogeneity and smooth surface. In addition, the TEM image depicted in Figure 5 show a honeycomb porous structure which is the result of hexagonal packing of unidimentional cylindrical pores. The ordered hexagonal array was further confirmed by the X–ray diffractogram shown in Figure 6 with four Bragg reflections that can be indexed as (100), (110), (200) and (210) typical of hexagonal p6mm configuration. The intense reflection that corresponds to the (100) diffraction peak with d = 45.5A° gives a lattice constant (pore centre distance) of α_o = 52.5A°estimated by the hexagonal unit cell relation (α_o = 2d$_{100}$/$\sqrt{3}$).

The specific surface area estimated with the standard BET method was 980m^{2}g^{-1} with a measured mesoporous volume of 0.65cm^{3}g^{-1} and a narrow pore size distribution centred at 2.9nm. As depicted in Figure 7 the nitrogen–adsorption of the prepared MCM–41 is a typical IV–isotherm of mesoporous materials with a step in the range of P/P$_o$ =
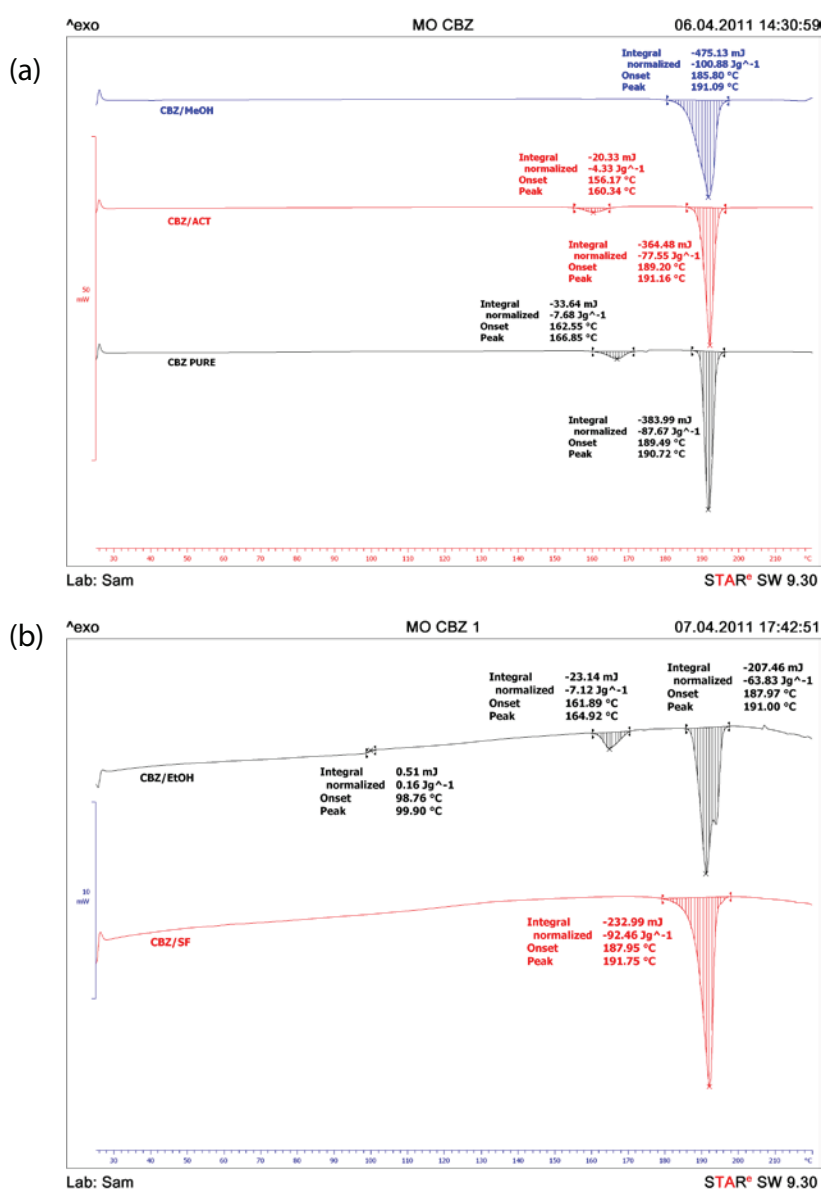

Figure 9: DSC thermograms of a) CBZ loaded MCM – 41 nanoparticles process by acetone, methanol – pure CBZ (bottom) and b) ethanol and control (processed only with CO$_2$).
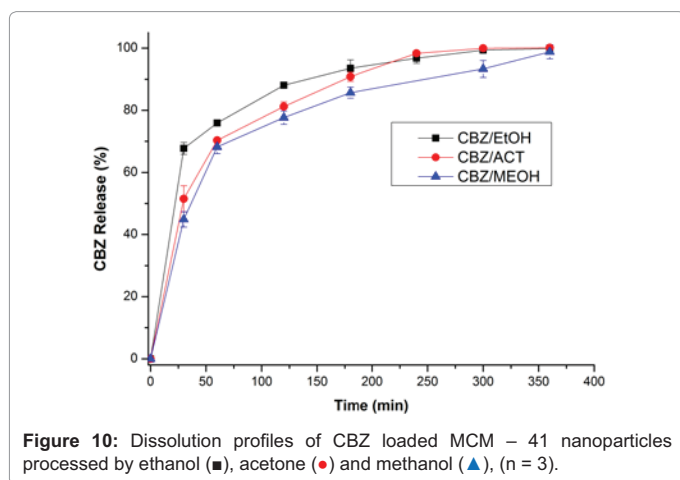
Figure 10: Dissolution profiles of CBZ loaded MCM – 41 nanoparticles processed by ethanol (■), acetone (●) and methanol (▲), (n = 3).
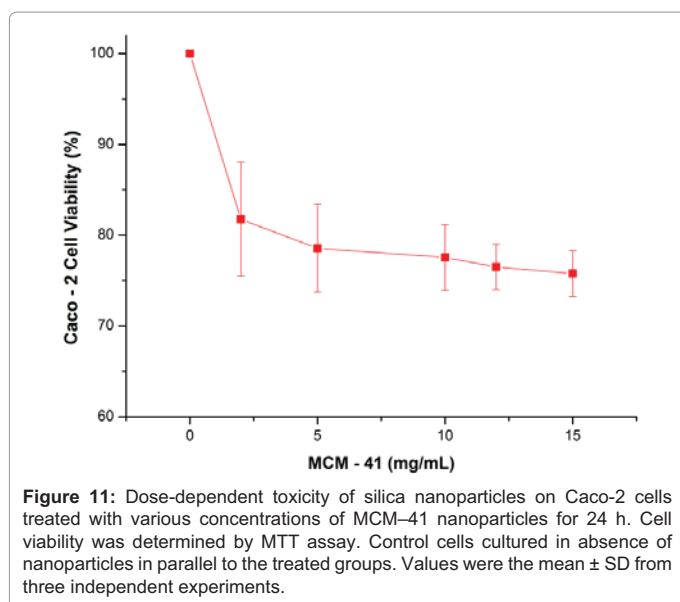

Figure 11: Dose-dependent toxicity of silica nanoparticles on Caco-2 cells treated with various concentrations of MCM–41 nanoparticles for 24 h. Cell viability was determined by MTT assay. Control cells cultured in absence of nanoparticles in parallel to the treated groups. Values were the mean ± SD from three independent experiments.

on previous studies [5] where CBZ showed high dissolving capacity within these solvents. The SF loading parameters were kept unchanged in order to investigate the solvent effect on CBZ encapsulation and the obtained crystalline state.

During the loading process the active molecules diffuse in the MCM–41 channel pores and onto the outer surface. As mentioned above the pore size of the MCM–41 is approximately 3nm and large enough to host the loaded material. The SF loading process revealed substantial drug loading (DL) efficiency (Table 2) for all solvents varying from 27–33% in descending order EtOH>ACT>MeOH.

Physicochemical characterisation

The produced CBZ/MCM–41 loaded powders were fully characterized by X-ray and DSC studies in order to determine CBZ crystalline state within the pore channels. It is known that CBZ polymorphs can be obtained upon crystallization from various solvent [27]. Thus, it is important to investigate the influence of the solvents on the CBZ crystal habits. The intensity peak positions and the relative intensities of pure CBZ and loaded samples are shown in Table 1. As it can also be seen from Figure 8 (a, b) the diffractogram of pure CBZ corresponds to form III (*P*–monoclinic) and they are in a good agreement with the results published by Rustichelli et al. [28]. Similarly the X–ray diffractograms of the samples processed with EtOH>MeOH>ACT correspond to form III>form II>form III respectively. However, the intensities of the measured samples vary, especially for forms I and II, compared to previous studies [28,29]

*CBZ/CO$_2$ (Form I)		**CBZ/MeOH (Form II)		**CBZ/ACT (Form III)		CBZ pure (Form III)	
2θ	Intensity (%)	2θ	Intensity (%)	2θ	Intensity (%)	2θ	Intensity (%)
10.10	4.47	5.02	100	5.00	35.51	12.69	21.35
13.08	91.83	8.66	35.25	8.66	18.75	13.00	48.17
13.65	25.77	12.25	68.61	13.08	100	13.58	100
14.16	27.39	13.23	9.70	13.33	24.60	14.10	30.02
15.04	100	18.38	12.42	14.14	28.30	14.94	48.26
15.29	94.58	20.10	46.28	14.98	42.48	15.30	90.56
15.82	52.65	24.40	19.70	15.27	85.55	15.78	59.16
18.69	40.56			15.83	52.25	18.56	30.10
19.55	50.34			18.67	35.20	19.36	51.21
20.34	23.90			19.46	48.10	20.29	29.38
23.36	22.44			20.05	26.40	23.35	29.21
23.87	29.19			23.34	22.00	23.87	39.38
24.94	44.97			23.85	30.78	24.75	33.40
26.65	23.31			24.90	37.55	27.49	85.88
27.19	39.80			26.67	30.74		
27.54	39.75			27.60	47.01		

*sample processed with only CO$_2$ (control), **samples processed with CO$_2$ and various solvents

Table 1: Powder X-ray Diffraction peak positions and relative intensities of the anhydrous polymorphs of CBZ produced after supercritical processing with various organic solvents.

0.3–0.4 which is typical for the filling of mesoporous systems. The thickness of the pore wall can be estimated by the difference between the pore centre distance and the pore diameter. The estimated wall thickness [12] can be estimated from the difference the pore distance and the mean mesopore width ($d_{pore\ wall} = a_0 - W_{BJH}$) and it was found 2.4nm.

Carbamazepine inclusion into MCM–41

The synthesized MCM–41 nanoparticles presented high specific surface area and pore volume in order to achieve the highest possible drug loading [6]. The tree main methods reported for the drug inclusion in mesoporous silica nanoparticles are the solvent method, the impregnation method and the melt method [23]. In the current study we report for first time the use of supercritical CO$_2$ for the inclusion of active substances within the silica pores. The employment of supercritical fluids is advantageous compared to the previous methods because it is one step process, facilitates high drug loading, removes un–trapped drug during depressurization and loaded silica nanoparticles are obtained in a powder form.

Carbamazepine was dissolved in acetone or methanol prior supercritical fluid processing. The selection of the solvents was based

Samples	Peak 1 (°C)	Peak 2 (°C)	Peak 3 (°C)	ΔH (Jg⁻¹)	Loading (%)
Control (CO$_2$)	-	-	191.75	-92.46	-
CBZ pure	-	166.85	190.72	-87.67	-
CBZ/ACT	-	160.34	191.16	-77.55	31.5
CBZ/MeOH	-	-	191.09	-100.88	27.4
CBZ/EtOH	99.90	164.92	191.00	-63.83	33.2

Table 2: Transition Temperatures, enthalpy of melting, and drug loading of CBZ samples.

because of the preferred orientations of samples in the powder X–ray analysis.

Figure 9 (a, b) shows the DSC thermograms of pure CBZ and MCM – 41 loaded samples. Previous studies demonstrated that CBZ exhibits enantiotropic polymorphism, which means a transition temperature can be observed below the melting point of either of the polymorphs at which both these forms have the same free energy. Above the transition temperature, the higher melting form (I) has the lower free energy and is more stable. According to other researchers [27,28] the DSC thermograms of CBZ form III shows two endotherms where the first endotherm is present in the range 160–175°C and is not followed by any exothermic event while a sharp endotherm occurs at the range 189–192°C. The thermogram of pure CBZ showed a small melting endotherm at 166.67°C followed by a second endotherm at 191.67°C. These two endotherms correspond to form III and I of CBZ, respectively. The melting endotherm at 191.67°C indicates that the used CBZ herein was form III.

Interestingly, CBZ/MCM – 41 samples processed with ACT or EtOH showed the presence of CBZ form III and I respectively (Table 2). The CBZ form I have been reported before [28] and show a single endothermic peak approximately at 192°C. In contrast, samples processed with EtOH showed an exothermic peak at 99.90°C followed by a melting endotherm at 191.67°C that corresponds to the trigonal form II. The presence of the exothermic peak in the range of 80 – 100oC is typical for CBZ polymorph II due to the presence of amorphous sample crystalling during DSC [28]. The DSC traces and also the melting points depend on the heating rates and thus they could be slightly different to those reported in literature. It is obvious that the nature of the solvent used in combination to super CO_2 affects CBZ crystalline state. The influence of CO_2 was also investigated by processing equal amounts of CBZ powder under the same experimental settings. The results indicate that the obtained CBZ powder was in form I as shown in Figure 9b. It is obvious that CO_2 can alter CBZ crystal habit. The DSC thermograms are in agreement with the X–ray studies and confirm the previous observations. In conclusion, the above studies showed that solvents play a key role on the crystalline state of polymorphic active substances when co-processed with supercritical CO_2.

Dissolution studies

The dissolution profiles of CBZ/MCM - 41 loaded nanoparticles were investigated under sink conditions (C<0.2 Cs). As shown in Figure 10 all samples demonstrated increased CBZ dissolution profiles with more than 65% of the active been released after 60 min. The release percentage where found to depend on the actual drug loading. As it can be seen in Figure 8 the MCM–41 nanoparticles with the higher CBZ loading demonstrated faster dissolution rates. The encapsulation of water insoluble drugs within the pore channels of silica nanoparticles facilitated efficient drug particle size reduction and hence improved dissolution rates. As mentioned above the average pore diameter is approximately 2.9 nm which means that the particle size of the encapsulated CBZ is smaller than the pore diameter. In addition, the rapid dissolution profiles can be explained by the displacement desorption of CBZ by the influx of water [30]. In this case the encapsulated CBZ is desorbed by competitive adsorption of water molecules on the hydrophilic silica surface. We also assumed that CBZ did not interact with silanol groups that could retard the drug dissolution as it has been previously reported [31]. The increased dissolution profiles and the CBZ loading efficiency are of particular interest for pharmaceutical applications in order to improve the delivery of poorly soluble drugs and consequently increasing drug

absorption and bioavailability. For Class II active substances the dissolution rate is the limiting factor to adsorption.

Cell cytotoxicity

In the last decade, silica nanoparticles have been widely used for various biopharmaceutical applications and in many occasions have been found to induce cytotoxicity in cell culture lines [32].In these studies it was demonstrated that cell cytotoxicity depends on the actual particle size of the silica nanoparticles. In our studies we conducted MTT cytotoxicity assays using Caco–2 cells. As it can be seen in Figure 11 the MCM–41 demonstrated relatively low cytotoxicity and at high concentrations (15mg/ml) cell viability was above 75%. Although additional studies are required to prove the safety of MCM – 41, recent studies [33] showed that low *in vitro* cytoxicity is a good indication for *in vivo* biocompatibility. As a result MCM–41 nanoparticles could be effectively used asa drug delivery systems for oral administration of active substances.

Conclusions

In the current study we synthesized MCM–41 nanoparticles with high surface area and narrow pore size for the encapsulation of a major antiepileptic active substance. The encapsulation was carried out by implementing supercritical CO_2 process in combination with various solvents. The results demonstrated that SF processing increased drug loading while drug encapsulation in silica nanoparticles enhanced dissolution rates. It was also demonstrated that co–processing with various solvents influences CBZ crystalline state depending on the solvent nature. The MTT assay studies of Caco–2 cells indicated low cytotoxicity at high MCM–41 nanoparticle concentrations. In conclusion, SF can be successfully employed for the delivery of active substances using MCM–41 nanoparticles.

Declaration of Interest

The authors report no conflicts of interest. The authors alone are responsible for the content and writing of this article.

References

1. Kresge CT, Leonowicz ME, Roth WJ, Vartuli JC, Beck JS (1992) Ordered mesoporous molecular sieves synthesized by a liquid-crystal template mechanism. Nature 359: 710-12.

2. Huo Q, Margoleses SI, Ciesla U, Feng UP, Gier DE, et al. (1994) Generalized synthesis of periodic surfactant/inorganic composite material. Nature 368: 317-320.

3. Beck JS, Vartuli JC, Roth WJ, Leonowicz ME, Kresge CT, et al. (1992) A new family of mesoporous molecular sieves prepared with liquid crystal templates. J Am Chem Soc 114: 10834 – 43.

4. Vallet-Regi M, Ramila A, Del Real RP, Perez-Pariente J (2001) A new property of MCM-41: Drug delivery system. Chem Mater 13: 308–311.

5. Thomas MJ, Slipper I, Walunj A, Jain A, Favretto ME, et al. (2010) Inclusion of poorly soluble drugs in highly ordered mesoporous silica nanoparticles. Int J Pharm 387: 272-7.

6. Slowing II, Vivero-Escoto JL, Wu CW, Lin VS (2008) Mesoporous silica nanoparticles as controlled release drug delivery and gene transfection carriers. Adv Drug Deliv Rev 60: 1278-88.

7. Liong M, Lu J, Kovochich M, Xia T, Ruehm SG, et al. (2008) Multifunctional inorganic nanoparticles for imaging, targeting, and drug delivery. ACS Nano 2: 889-96.

8. Vallet-Regi M, Balas F, Arcos D (2007) Mesoporous Materials for Drug Delivery. Angew Chem Int Ed 46: 7548-58.

9. Wen LX, Ding HM, Wang JX, Chen JF (2006) Porous hollow silica nanoparticles as carriers for controlled delivery of ibuprofen to small intestine. J Nanosci Nanotechnol 9-10: 3139-44.

10. Qu F, Zhu G, Huang S, Li S, Zhang JSD, et al. (2006) Controlled release of Captopril by regulating the pore size and morphology of ordered mesoporous silica. Microporous and Mesoporous Materials 92:1–9.

11. Heikkilä T, Salonen J, Tuura J, Kumar N, Salmi T, et al. (2007) Evaluation of Mesoporous TCPSi, MCM-41, SBA-15, and TUD-1 materials as API carriers for oral drug delivery. Drug Deliv 14: 337–347.

12. Huh S, Wiench JW, Yoo JC, Pruski M, Lin VSY (2003) Organic Functionalization and Morphology Control of Mesoporous Silicas via a Co-Condensation Synthesis Method. Chem. Mater. 15: 4247–4256.

13. Cagnol F, Grosso D, Sanchez C (2004) A General One-pot Process Leading to Highly Functionalised Ordered Mesoporous Silica Films. Chem Commun 1742–1743.

14. Han L, Sakamoto Y, Terasaki O, Li Y, Che S (2007) Synthesis of Carboxylic Group Functionalized Mesoporous Silicas (CFMSs) with Various Structures. J Mater Chem 17: 1216–1221.

15. Lu J, Liong M, Zink JI, Tamanoi F (2007) Mesoporous silica nanoparticles as a delivery system for hydrophobic anticancer drugs. Small 3: 1341-6.

16. He Q, Shi J, Chen F, Zhu M, Zhang L (2010) An anticancer drug delivery system based on surfactant-templated mesoporous silica nanoparticles. Biomaterials 31: 3335-46.

17. Smirnova I, Suttiruengwong S, Arlt W (2004) Feasibility study of hydrophilic and hydrophobic silica aerogels as drug delivery systems. J Non-Cryst Solids 350: 54-60.

18. Gorle BSK, Smirnova I, Dragan M, Dragan S, Arlt W (2008) Crystallization under supercritical conditions in aerogels. J. Supercrit. Fluids 44: 78–84.

19. Gorle BSK, Smirnova I, McHugh MA (2009) Adsorption and thermal release of highly volatile compounds in silica aerogels. J Supercrit Fluids 48: 85-92.

20. Gorle BSK, Smirnova I, Arlt W (2010) Adsorptive crystallization of benzoic acid in aerogels from supercritical solutions. J Supercrit Fluids 52: 249-257.

21. Amidon GL, Löbenberg R (2000) Modern bioavailability, bioequivalence and biopharmaceutics classification system. New scientific approaches to international regulatory standards. Eur J Pharm Biopharm 50: 3–12.

22. Amidon GL, Lunnernas H, Shah VP, Crison JR (1995) A theoretical basis for a biopharmaceutic drug classification: the correlation of *in vitro* drug product dissolution and *in vivo* bioavailability. Pharm Res 12: 413–420.

23. Mellaerts R, Jammaer JA, Speybroeck MV, Chen H, Humbeeck JV, et al. (2008) Physical state of poorly water soluble therapeutic molecules loaded into SBA-15 ordered mesoporous silica carriers: a case study with itraconazole and ibuprofen. Langmuir 24: 8651-9.

24. Mosmann T (1983) Rapid calorimetric assay for cellular growth and survival: application to proliferation and cytotoxicity assays. J Immunol Methods. 65: 55-63.

25. Kim JH, Yoon SB, Kim JY, Chae YB, Yu JS (2008) Synthesis of monodisperse silica spheres with solid core and mesoporous shell: Morphological control of mesopores. Colloids and Surfaces A: Physicochem. Eng. Aspects 313–314: 77–81.

26. Fedorenko SV, Bochkova OD, Mustafina AR, Burilov VA, Kadirov MK, et al. (2010) Dual visible and near-infrared luminescent silica nanoparticles. Synthesis and aggregation stability. J Phys Chem C 114: 6350–6355

27. Grzesiak AL, Lang M, Kim K, Adam J, Matzger AJ (2003) Comparison of the Four Anhydrous Polymorphs of Carbamazepine and the Crystal Structure of Form I. J Pharma Sci 92: 2260 – 71.

28. Rustichelli C, Gamberini G, Ferioli V, Gamberini MC, Ficarra R, et al. (2000) Solid-state study of polymorphic drugs: carbamazepine. J Pharm Biomed Anal. 23: 41-54.

29. Katzhendler I, Friedman RM (1998) Crystalline properties of carbamazepine in sustained release hydrophilic matrix tablets based on hydroxypropyl methylcellulose. J Controlled Rel 54: 69–85.

30. Mellaerts R, Aerts CA, Van Humbeeck J, Augustijns P, Van den Mooter G, et al. (2007) Enhanced release of itraconazole from ordered mesoporous SBA-15 silica materials. Chem Commun 1375–1377.

31. Horcajada P, Ramila A, Perez-Pariente J, Vallet-Regi M (2004) Influence of pore size of MCM-41 matrices on drug delivery rate. Micropor Mesopor Mater 68: 105 – 109.

32. Lin WS, Huang YW, Zhou XD, Ma YF (2006) *In vitro* toxicity of silica nanoparticles in human lung cancer cells. Toxicol Appl Pharmacol 217: 252–259.

33. Li L, Tang F, Liu H, Liu T, Hao N, et al. (2010) *In vivo* delivery of silica nanorattle encapsulated docetaxel for liver cancer therapy with low toxicity and high efficacy. ACS Nano 4: 6874-82.